Journal of Cleaner Production 462 (2024) 142643

Contents lists available at ScienceDirect

Journal of Cleaner Production

journal homepage: www.elsevier.com/locate/jclepro

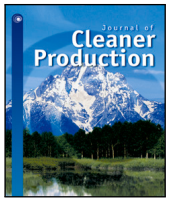

The impact of heat pump load flexibility on its process integration and economics

Jasper V.M. Walden *, Panagiotis Stathopoulos

German Aerospace Center (DLR), Institute of Low-Carbon Industrial Processes, Simulation and Virtual Design, Walther-Pauer-Straße 5, Cottbus, 03046, Brandenburg, Germany

ARTICLE INFO

Handling Editor: Cecilia Maria Villas Bôas de Almeida

Keywords:
Dynamic Pinch Analysis
Industrial heat pump integration
Non-continuous industrial processes
Part load heat pump model
Heat pump load flexibility
Time-resolved industrial process data

ABSTRACT

The conventional methodology of heat pump integration has found application in various industries, including cheese production, spray drying, milk evaporation systems, brewing, and meat processing. While several approaches have been developed for optimizing direct and indirect heat recovery in non-continuous industrial processes, the optimal integration of heat pumps in non-continuous processes remains a challenge.

This paper introduces a systematic methodology that leverages extensive datasets of time-resolved industrial process data to determine the optimal heat pump integration and the level of heat pump load flexibility that maximizes the economic benefit. Thus, the work establishes a connection between the domain of Process Integration and heat pump load flexibility. Additionally, the study provides insights on the requirements for load flexibility during the design phase of the heat pump, offering an estimation on the need for research on heat pump flexibility.

The findings indicate the presence of a load flexibility threshold in the examined case study, beyond which additional load flexibility yields diminishing returns. Furthermore, the study shows that different heat pump integration parameters are chosen based on the heat pump's capability for load flexibility. Within the investigated case, a heat pump with a minimum load of 55% increases the net present value by 19.3% compared to a load inflexible heat pump.

1. Introduction

The urgency for a rapid transition to a low-carbon industry is evident. Although a clear path for the electrification of process heat has yet to be determined, a consensus exists within the scientific community that industrial, large-scale heat pumps will play a significant role in this transition (IEA HPT Annex 58, 2023). For example, a large variety of reviews regard the potential for decarbonization by heat pumps. Such as Kosmadakis (2019) who estimate the potential for decarbonization by industrial heat pumps. Madeddu et al. (2020) show the potential of decarbonization by electrification. Zühlsdorf et al. (2019a) investigated the technologies and potentials for heat supply above 150 °C. Furthermore, the underlying economics of large scale heat pumps have been examined by Schlosser et al. (2020), while Marina et al. (2021) gave an overview of the heat pump market potential. The European Commission conducted a study on Policy Support for Heating and Cooling Decarbonization (Gerard et al., 2021), which regards heat pumps as an essential part for decarbonizing the heat supply. Research on common faults of large scale heat pumps was carried out by Aguilera et al. (2022). Jiang et al. (2022) reviewed the technology of high temperature heat pumps. A thorough review on transcritical heat pump cycles for industrial application was carried out by Adamson et al. (2022). However, a key challenge to the widespread adoption of heat pumps lies in the identification of their optimal integration parameters within non-continuous industrial process as this influences economic and environmental feasibility substantially.

1.1. State of the art

The systematic, thermodynamic approach to heat pump integration in industrial processes was first developed by Townsend and Linnhoff (1983). The methodology has been applied to various industries such as cheese production (Becker et al., 2012), spray drying (Schlosser et al., 2023; Walmsley et al., 2017), milk evaporation systems (Lincoln et al., 2022), brewing (Eiholzer et al., 2017) and meat processing (Klinac et al., 2023).

Several approaches have been developed to optimize direct and indirect heat recovery for non-continuous process. However, heat pump integration in a non-continuous process is particularly challenging.

* Corresponding author.
E-mail address: jasper.walden@dlr.de (J.V.M. Walden).

https://doi.org/10.1016/j.jclepro.2024.142643
Received 20 February 2024; Received in revised form 19 April 2024; Accepted 20 May 2024
Available online 24 May 2024

Nomenclature

Acronyms

aCOP	Annualized mean coefficient of performance
CAPEX	Capital expenditure
COP	Coefficient of performance
CU	Cold utility
DLR	German Aerospace Center
GCC	Grand Composite Curve
HEx	Heat exchanger
HP	Heat pump
HU	Hot utility
ISSP	Indirect source-sink profiles
LMTD	Log. mean temperature difference
NPV	Net present value
OPEX	Operational expenditure
PLF	Part load factor
PLR	Part load ratio
PR	Pressure ratio
R	Cash flow

Latin symbols

$\bar{p}$	Optimization variables
$\dot{m}$	Mass flow
$\dot{Q}$	Heat flow rate
a	Function coefficient
b	Coil pitch
C	Correlation constant
c	Cost
D	Diameter
E	Cost function exponent
f	Cost function factor
h	Enthalpy
i	Discount rate
k	Overall heat transfer coefficient
N	Number of years
n,m	Correlation exponents
Nu	Nusselt Number
P	Wetted perimeter
Pr	Prandtl Number
Q	Heat
R	Cash flow
r	Curvature radius
Re	Reynolds Number
s	Operational cost savings
T	Temperature
u	Fluid velocity
W	Work

Greek symbols

α	Individual convection heat transfer coefficient
Δp	Pressure drop
δ	Degradation factor
η	Efficiency
γ	Dimensionless pitch
γ	Function coefficient
λ	Thermal conductivity
μ	Dynamic viscosity
ρ	Density

Subscripts

boiler	Boiler
carnot	Carnot
comp	Compressor
cov	Heat coverage by heat pump
d	Design
el	Electricity
fuel	Fuel
h	hydraulic
ideal	Ideal heat pump
inv	Investment
is	Isentropic
Lang	Lang factor
lb	Lower bound
lifetime	Lifetime
lift	Lift
min	Minimum
om	Operating and maintenance
pi	Planning and installation
PL	Part load
sink	Heat sink side of the heat pump
source	Heat source side of the heat pump
sys	System integration and peripherals

Stampfli et al. (2019) demonstrated the integration of a heat pump storage system into a non-continuous process by a hybrid approach, combining mathematical optimization and Pinch Analysis. Agner et al. (2022) proposed a graphical approach based on the indirect-source-sink-profiles (ISSPs) used in thermal energy storage (TES) integration (Olsen et al., 2017). A superstructure optimization to simultaneously integrate a thermal energy storage and heat pump into a multi-period industrial process was carried out by Prendl et al. (2021).

Furthermore, the investigation of the capacity for load flexibility in industrial processes and heat pump systems is a focal point of research (Sadjjadi et al., 2023). Walden et al. (2023a) explored the potential of a heat pump heat storage system to smoothen fluctuations in energy supplied by renewable generation. The integration of electricity and heating sectors using heat pumps to efficiently produce heat and offer demand flexibility has been investigated by Meesenburg et al. (2018). Padullés et al. (2023) showed that load shifting by a heat pump storage system improves its business case significantly.

The existent literature demonstrates the advantageous impact of heat pump integration and heat pump load flexibility on economic viability and the reduction of greenhouse gas emissions. The work by Ghaderi et al. (2023) and Walden et al. (2023b) have used dynamic process data to lever more insights from Pinch Analysis and derived Dynamic Pinch Analysis. However, none of these studies have successfully merged the appropriate process integration of a heat pump with an evaluation of the impact of the heat pump's load flexibility, aiming to achieve the most economically efficient heat pump integration.

By the application of Pinch Analysis and dynamic process data, a methodology is developed to investigate the economic advantages of heat pump load flexibility and the optimal degree of heat pump load flexibility. In this method, the optimal heat pump integration, including heating capacity and temperatures, is determined, along with the level of heat pump load flexibility, at which the economic improvement is maximized.

1.2. Research objective

The precursor study (Walden et al., 2023b) showed that heat pump integration can be significantly improved by leveraging dynamic process data via mathematical optimization. In comparison to the conventional time-average-method approach, the method determined that a 33% smaller heat pump can cover more operating cases and provide larger cost and energy savings with the net present value (NPV) and internal rate of return (IRR) being more than tripled. The study investigated 8759 time slices of process data and employed mathematical optimization to find the heat pump integration with the highest NPV or IRR. Nonetheless, a previous assumption restricted the heat pump to operate solely under full load conditions. The current work aims to analyse the improvement in performance that could be achieved through heat pump load flexibility.

By gradually increasing the load flexibility of the heat pump, the effects on its integration parameters (T_{sink}, T_{source}, $\dot{Q}_{\text{sink}}$) and the impact on the value of the investment are investigated. Furthermore, an optimal degree of heat pump flexibility is determined for a case study.

In order to study these effects, a reduced-order heat pump part load model is required. An extension to the Carnot model to account for part load is proposed in Section 2. Consequently, Section 3 explains dynamic heat pump integration, the underlying optimization problem and the economic evaluation.

The study addresses the following research questions:

- Which modelling approaches can be employed to characterize the part load efficiency of a heat pump?
- What is the optimal level of load flexibility for an industrial heat pump from a thermo-economic perspective?
- To what extent does the load flexibility of a heat pump influence its integration parameters (T_{sink}, T_{source}, $\dot{Q}_{\text{sink}}$, COP) and heat coverage?

2. Heat pump modelling

Heat pump models are usually derived through basic thermodynamic relations. Eq. (1) describes the energy balance of a heat pump.

$$\dot{Q}_{\text{sink}} = \dot{Q}_{\text{source}} + W_{\text{HP}} \tag{1}$$

The coefficient of performance (COP) of a heat pump is the ratio of supplied heat flow rate to work input required (Eq. (2)). Higher COPs represent a higher efficiency and lower power consumption.

$$\text{COP}_{\text{d}} = \frac{\dot{Q}_{\text{sink,d}}}{W_{\text{HP}}} \tag{2}$$

A common approach to estimate the COP of a heat pump is the application of a constant 2nd law efficiency η_{carnot} as a coefficient to the maximum theoretical efficiency, as depicted in Eq. (3).

$$\text{COP}_{\text{d}} = \eta_{\text{carnot}}\text{COP}_{\text{ideal}} = \eta_{\text{carnot}}\frac{T_{\text{sink}}}{T_{\text{sink}} - T_{\text{source}}} \tag{3}$$

The Carnot efficiency is defined by:

$$\eta_{\text{carnot}} = \frac{\text{COP}_{\text{d}}}{\text{COP}_{\text{ideal}}}. \tag{4}$$

By combining Eqs. (1) and (2) a relation for the heat load supplied by the heat pump as a function of the COP and heat source heat load is derived (Eq. (5)).

$$\dot{Q}_{\text{sink}} = \frac{\text{COP} \cdot \dot{Q}_{\text{source}}}{\text{COP} - 1} \tag{5}$$

Through the utilization of Eqs. (1)–(5), a suitable reduced-order heat pump model that relies on thermodynamic principles can be derived. However, this model is not suitable for part load of the heat pump. The following section extends the model for part load operation.

2.1. Part load heat pump model

The previously outlined thermodynamic model is extended to account for changes in efficiency during part load operation of the heat pump.

For chillers or commercial heat pumps, international standards estimate a part load COP using a correction parameter known as the partial load factor (PLF), which acts as a multiplier to the design condition COP (Eq. (6)).

$$\text{COP}_{\text{PL}} = \text{PLF} \cdot \text{COP}_{\text{d}} \tag{6}$$

For example, the AHRI standard 210/240 (AHRI - Air-Conditioning, Heating, and Refrigeration Institute, 2020) determines the partial load factor by use of a degradation coefficient (Eq. (7)), typically established experimentally.

$$\text{PLF} = 1 - \delta(1 - \text{PLR}) \tag{7}$$

With the part load ratio (PLR) as the ratio between part load heat flow rate and design heat flow rate of the heat pumps heat sink.

$$\text{PLR} = \frac{\dot{Q}_{\text{sink,PL}}}{\dot{Q}_{\text{sink,d}}} \tag{8}$$

However, the approach provides only a linear relation of the COP in part load.

This work creates a heat pump model based of the individual components part load behaviour. It is assumed, that the heat pumps load is controlled by the compressor power. Furthermore, we assume a positive displacement compressor and thus, the condenser and evaporator temperatures can be kept at the same levels in part load. Consequently, by alternating the compressor power, the heat pump cycles mass flow is reduced. Varying the compressor power is equivalent with regulating the heat pump's load by control of the rotational speed of the compressor. As a result, the changes in component performance are mainly dependent on the mass flow.

In order to create a reduced order heat pump part load model, a part load efficiency factor η_{PL} is introduced.

$$\text{COP}_{\text{PL}} = \eta_{\text{carnot}} \cdot \text{COP}_{\text{ideal}} \cdot \eta_{\text{PL}} \tag{9}$$

The part load efficiency factor η_{PL} is determined by dividing the part load COP by design COP.

$$\eta_{\text{PL}}(\text{PLR}) = \frac{\text{COP}_{\text{PL}}}{\text{COP}_{\text{d}}} \tag{10}$$

The part load COP is determined by the part load heat sink heat load and the part load compressor power (11). It should be noted, that the inefficiencies of the electric motor are neglected. In order to determine the parameters of the part load COP, the part load behaviour of the heat pump cycles components have to be modelled and investigated. The next section breaks down the component models within a standard vapour compression cycle heat pump, as shown in Fig. 4.

$$\text{COP}_{\text{PL}} = \frac{\dot{Q}_{\text{sink,PL}}}{W_{\text{comp,PL}}} \tag{11}$$

2.1.1. Component modelling

Heat exchangers. The heat exchangers partial heat loads are modelled by a factor f_{kA} which scales the product of overall heat transfer coefficient and area kA based on the mass flow within the condenser.

$$\dot{Q}_{\text{sink,PL}} = \dot{m}_{\text{in,1}} \cdot (h_{\text{out,1}} - h_{\text{in,1}}) \tag{12}$$

$$= -kA \cdot f_{\text{kA}}(\dot{m}_{\text{HP}}) \cdot LMTD \tag{13}$$

The factor f_{kA} is determined by two factors, f_1 and f_2, which represent the change in heat transfer coefficient of the respective fluids on each side of the heat exchanger.

$$f_{\text{kA}} = \frac{k_{\text{PL}}}{k_{\text{nominal}}} = \frac{2}{\frac{1}{f_1(\dot{m}_{\text{HP}})} + \frac{1}{f_2(\dot{m}_{\text{HP}})}} \tag{14}$$

To derive a function f_i which represents the change in heat transfer by reduction of the mass flow, the occurring fluid dynamic effects need to be understood. When the mass flow is reduced, less fluid is in contact with the surface of the heat exchanger, which worsens the convective heat transfer process. Furthermore, the heat transfer coefficient strongly relies on the governing flow regime. The Reynolds number (Eq. (17)) is a dimensionless parameter used to characterize the flow regime. It is related to mass flow rate, fluid density, fluid velocity, and characteristic length. Thus, the Reynolds number often appears in heat transfer coefficient correlations as a key parameter. The hydraulic diameter (Eq. (15)) is applied as the characteristic length (Incropera, 2007). Combining Eqs. (15)–(17) yields a mass flow dependent Reynolds number as seen in the second part of Eq. (17).

$$D_h = \frac{4A}{P} \tag{15}$$

$$\dot{m} = \rho \cdot u \cdot A \tag{16}$$

$$\mathrm{Re} = \frac{\rho \cdot u \cdot D_h}{\mu} = \frac{4\dot{m}}{P\mu} \tag{17}$$

In summary, the specific relationship between mass flow rate and heat transfer coefficient depends on factors like flow regime, fluid properties, and geometrical configurations. As a result, there is not a universal equation that applies to all situations, and engineers often rely on experimental data and established correlations for their specific applications.

The majority of heat transfer coefficient estimations rely on the Nusselt number (Eq. (18)), wherein the Nusselt number is a function determined by the Reynolds and Prandtl numbers.

$$\alpha = \mathrm{Nu}(Re, Pr)\frac{\lambda}{L} \tag{18}$$

Correlations for the Nusselt number are typically expressed in the form of Eq. (19), as detailed by Incropera (2007). The widely used Dittus–Boelter correlation (Dittus and Boelter, 1985) for turbulent flow in smooth tubes is among these. An extensive overview of correlations is available in the work of Dorao and Fernandino (2017), with additional correlations found in references such as (Shah, 1979; Thome, 2005; Han et al., 2006).

$$\mathrm{Nu} = C\,Re^n\,Pr^m \tag{19}$$

Condenser. The current work is applying the correlation of Crosser (1955) to estimate the condensing heat transfer coefficient of the working fluid. Crosser et al. suggest to use C = 5.03, n = $\frac{1}{3}$ and m = $\frac{1}{3}$ in Eq. (19). Fig. 1 depicts the fit between the heat transfer coefficient used in TesPy (Witte and Tuschy, 2020) and the correlation of Crosser et al.

Shell-side fluid. The behaviour of the secondary side heat transfer coefficient is considered to be similar to shell-side heat transfer. A correlation (Eq. (20)) dependent on Reynolds- and Prandtl number was determined by Salimpour (2009) and is applied in this work.

$$\mathrm{Nu} = 19.64\,Re^{0.513}\,Pr^{0.129}\,\gamma^{0.938} \tag{20}$$

with

$$\gamma = \frac{b}{\pi D} \tag{21}$$

The characteristic dimensions of b = 17 mm and r = 60 mm given by Salimpour (2009) have been applied.

For reference, the commonly applied Dittus and Boelter (1985) correlation is illustrated in Fig. 2 with the correlations used in TesPy and the correlation of Salimpour et al.

Evaporator. Similarly to the condensation correlations, it is difficult to describe the heat transfer coefficient for evaporation throughout the full range of a tube with a singular value. Especially considering the fluid-specific effects, the effects caused by the change of liquid mass fraction and the ensuing two-phase flow pattern. However, a variety

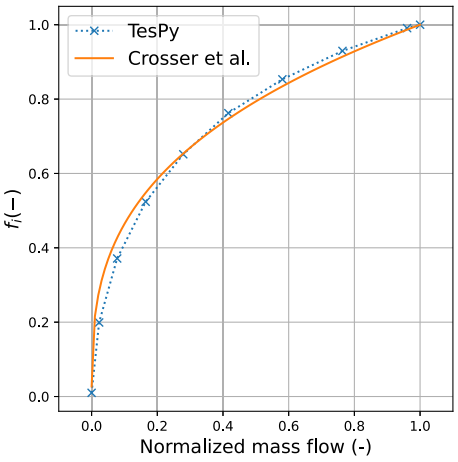

Fig. 1. Normalized heat transfer coefficient factor for a condensing fluid based on the correlation provided by Crosser (1955).

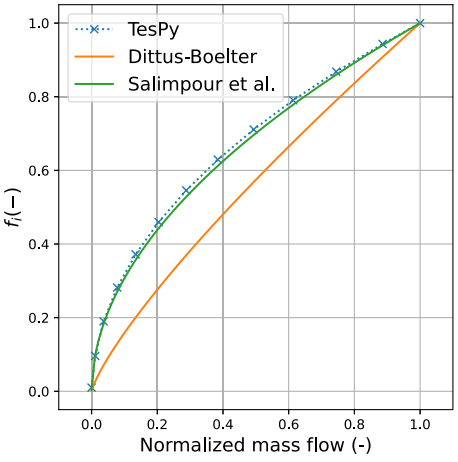

Fig. 2. Normalized heat transfer coefficient factor for a shell-side fluid.

of research (Lin et al., 2023; Ayub et al., 2019; Shah, 2021a,b) tried to address this issue by complex correlations. A very common one being the correlation by Chen (1966). This work applies the correlation provided within the TesPy framework (Witte and Tuschy, 2020).

Compressor. Eq. (22) describes the compressors energy balance. Typically, a constant isentropic efficiency is assumed to model a compressor. The current model is extended by a factor f_c which maps the change in isentropic efficiency in part load.

$$W_{comp} = (h_{out} - h_{in}) \cdot f_{comp}(\dot{m}_{HP}) \cdot \eta_{is,d} \tag{22}$$

Fig. 3 shows the normalized change in isentropic efficiency as the factor f_c. The orange line indicates the decrease in isentropic efficiency in a scroll compressor of a chiller as reported by Cecchinato (2010). A good fit with the characteristic given in TesPy is provided. It should be noted, that the efficiency line has been scaled to reach 1 at the design mass flow conditions. In this study, we applied the f_c characteristic provided by TesPy.

2.1.2. Reduced-order part load heat pump model

To determine the part load COP_{PL} and consequently the η_{PL} factor as described by Eqs. (10) and (11), the heat pump cycle and its components are simulated in TesPy. The applied cycle parameters can be found in Table 1. The part load calculation is conducted with the previously described characteristics. Furthermore, the heat exchangers

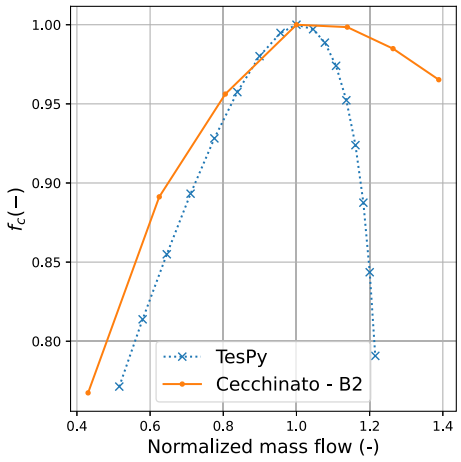

Fig. 3. Compressor part load efficiency factor.

Table 1
Heat pump cycle parameters.

Parameter	Value
$T_{source,in}$ (°C)	40
$T_{source,out}$ (°C)	35
$T_{sink,in}$ (°C)	70
$T_{sink,out}$ (°C)	80
η_s (%)	85
x_{c2} (-)	0
x_{c6} (-)	1
Δp_{HEx} (%)	1
$T_{approach,HEx}$ (K)	5
$\dot{W}_{comp}$ (kW)	200
PR_d (−)	3.59
p_{c1} (bar)	27.7

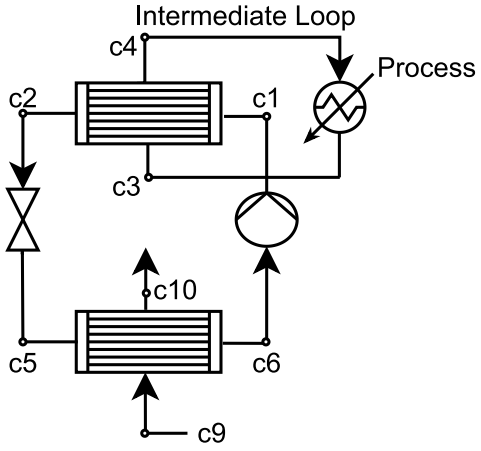

Fig. 4. The heat pump cycle of the reduced order heat pump model. The intermediate loop connecting the heat pump to the process is also visualized.

are modelled with an outlet to inlet pressure ratio of 0.99 in design condition. Changing the mass flow in heat exchangers will result in pressure drops. Thus, in part load, the pressure ratio will be replaced by a zeta function for all heat exchangers. The zeta value is geometry independent. The applied zeta function can be found in the documentation of TesPy.

Fig. 5 shows the change in part load heat pump efficiency η_{PL}. A quadratic decrease in efficiency is depicted, with an efficiency peak above 1 in off design conditions. Although, the peak does not exceed 0.4 %. This is explained by an increased heat transfer due to a decreased LMTD, which results in slightly higher heat uptake in the evaporator.

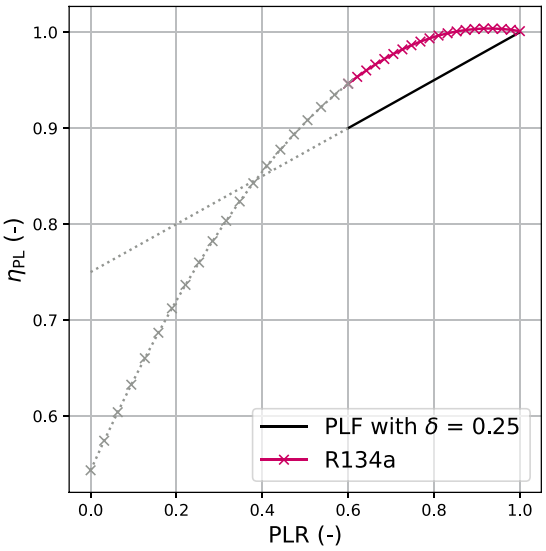

Fig. 5. Part load efficiency factor over part load ratio.

A similar behaviour is found in micro gas turbines (Li et al., 2020). This decreases the overall temperature difference and thus increases the COP. By lowering the PLR further, the influence of the decreased compressor efficiency prevails and the efficiency drops. Furthermore, the compressor exit temperature increases slightly as the compressor operates less efficiently in part load. The confluence of these factors contributes to the quadratic behaviour. Analogous behaviour in the part load operation of chillers has been documented in the work of Deymi-Dashtebayaz et al. (2019). The precise part load behaviour is specific to the working fluid. However, analysing the part load behaviour of different working fluids exceeds the scope of this paper. For detailed work on heat pump working fluid selection the reader is referred to the work of Zühlsdorf et al. (2019b,a).

Based on the presented results, a polynomial in the form of Eq. (23) is fitted to create a function for η_{PL}. In this work, R134a is applied. The coefficients are $a_1 = -0.535$, $a_2 = 0.992$, $a_3 = 0.543$. Fig. 5 shows the part load efficiency factor η_{PL}. The compressors part load characteristic is only defined until 55% of design mass flow. Thus, everything lower than 0.55 PLR is greyed out and depicted by the fitted polynomial.

$$\eta_{PL}(PLR) = a_1 PLR^2 + a_2 PLR + a_3 \tag{23}$$

3. Heat pump integration

Conventional heat pump integration methodology is conducted by use of the Grand Composite Curve (GCC). The GCC is a comprehensive representation of the thermal energy flows within an industrial process, aggregating the supply and demand profiles at different temperature levels. In the context of heat pump integration, the GCC serves as a crucial tool for identifying optimal temperature ranges and guiding the sizing and placement of heat pumps to maximize energy efficiency in industrial processes. The Appropriate Placement Principle, introduced by Townsend and Linnhoff (1983), states that a heat pumps heat sink has to be placed above the Pinch temperature, and the heat pumps heat source has to be placed below the Pinch temperature in order to achieve a system improvement. Fig. 6(a) shows a correct heat pump integration by application of the Appropriate Placement Principle to the GCC. In Fig. 6(b) the heat pump is correctly integrated, however, the heat pump violates the process demands depicted by the GCC. This means, the heat pump supplies more heat at the heat sink temperature T_{sink} than required by the process.

$$COP > \frac{c_{el}}{c_{fuel}/\eta_{boiler}}. \tag{24}$$

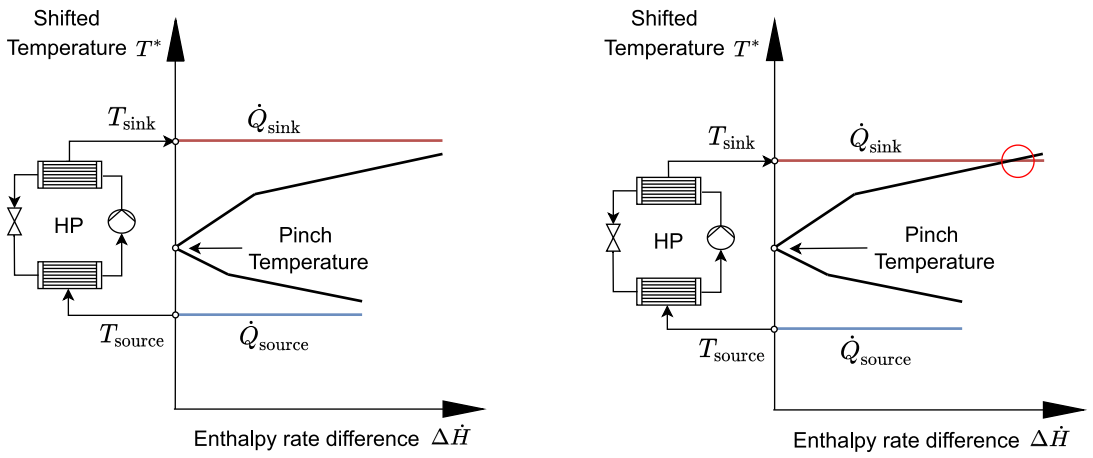

Fig. 6. Visualization of heat pump integration by Pinch Analysis. (a) demonstrates the correct integration across the Pinch Temperature. (b) shows an integration across the Pinch but with a temperature crossover between the heat supply by the heat pumps heat sink and the process heat demand.
Source: The Figures are taken from the authors previous work (Walden et al., 2023b).

The upper limit for the economically achievable temperature lift and thus the lower limit of the COP of a heat pump is constrained by the ratio of cost of electricity to reference fuel (Eq. (24)) as described by Schlosser et al. (2019). An increase in temperature lift leads to a decrease in COP (Eq. (3)) and an increase in delivered heat by the heat pump. Thus, by conventional heat pump integration a trade off between a high COP and a high heat coverage by the heat pump must be found. The optimum is usually close to the lower limit of the COP defined by the cost ratios (Eq. (24)), however, this only considers operational expenditures.

Furthermore, the temperature difference between the heat pumps streams and the process streams is crucial for the heat pump integration. The minimum temperature difference must be maintained at all times to ensure heat transfer and consequently heat supply by the heat pump to the process. The minimum temperature $\Delta T_{min,hp}$ difference is calculated as proposed by Stampfli et al. (2019). The heat pump is assumed to be connected through an intermediate loop (Fig. 4). The heat transfer between the intermediate loop and the heat pump is assumed to require a lower temperature difference of $^3/_4\,\Delta T_{HEx}$, due to a higher heat transfer coefficient of latent heat transfer. Within the GCC, the temperatures are shifted by $^1/_2\,\Delta T_{HEx}$. Thus, the total required temperature difference between the heat pump and the GCC amounts to $^5/_4\,\Delta T_{HEx}$. With a ΔT_{HEx} of 5 K, $\Delta T_{min,hp}$ equals 6.25 K.

3.1. Dynamic heat pump integration

While conventional heat pump integration relies on a single or a handful of operating points to design a suitable and economic heat pump, Dynamic Heat Pump Integration relies on a full annual set of process data and can thus provide more insight in the correct choice of a heat pump. Thus, it can also predict the energy savings and monetary savings more accurately. The heat pump's main parameters (source temperature, sink temperature, sink heat load) are determined through mathematical optimization with the objective to maximize the benefit of the investment.

3.2. Optimization

Mathematical optimization is employed to address the challenge of sizing and placement of a heat pump and to exploit the advantages of Dynamic Heat Pump Integration.

Table 2
The bounds of the optimization variables.

	T_{source} (°C)	T_{sink} (°C)	$\dot{Q}_{source}$ (kW)
Bounds	[10, 40]	[41, 200]	[0, 2000]

The optimization problem is described in Eqs. (25)–(28). The objective is to maximize the NPV (Towler, 2012; Turton et al., 2012) within the investments lifetime.

$$\max_{\bar{p}} \quad \text{NPV} \tag{25}$$

$$\bar{p} = [T_{source}, T_{sink}, \dot{Q}_{sink}] \tag{26}$$

$$\text{s. t.} \quad \dot{Q}_{sink} \leq \dot{Q}_{hot,GCC} \tag{27}$$

$$\dot{Q}_{source} \leq \dot{Q}_{cold,GCC} \tag{28}$$

Table 2 depicts the applied bounds for the optimization variables. The optimization problem is solved by differential evolution (Storn and Price, 1997) with the SciPy optimization library (Virtanen et al., 2020).

Fig. 7 gives an overview of the calculation order within the optimization. Firstly, a feasibility check is performed, which includes the following parameters:

- Is heat below the pinch temperature available, which could serve as heat source?
- Is the lower bound of T_{source} smaller than $PT - \Delta T_{min,hp}$?
- Are the chosen T_{sink} and T_{source} above and below the PT, respectively?

If all the queries can be answered with a yes, the heat pump is feasible. Consequently, a value for PL is calculated. PL is the ratio of the heat load $\dot{Q}_{gcc}$ required by the process at temperature T_{sink} and the design heat load of the heat pump $\dot{Q}_{sink,d}$. This parameter indicates the extent to which the heat pump needs to operate in part load to remain operable. Thus, the PL parameter is equal to the PLR (Eq. (8)). Consequently, if PL is within the bound set by PL_{lb}, the heat pumps part load parameters are calculated based on the PLR and consequently, its residual utility load and operating cost. The part load lower bound PL_{lb} is slowly increased to constraint the heat pumps minimum relative load until it is only operable in full load (100%) conditions. This approach is akin to an ϵ-constraint method, employed to illustrate the influence of part load capability rather than merely incorporating it as

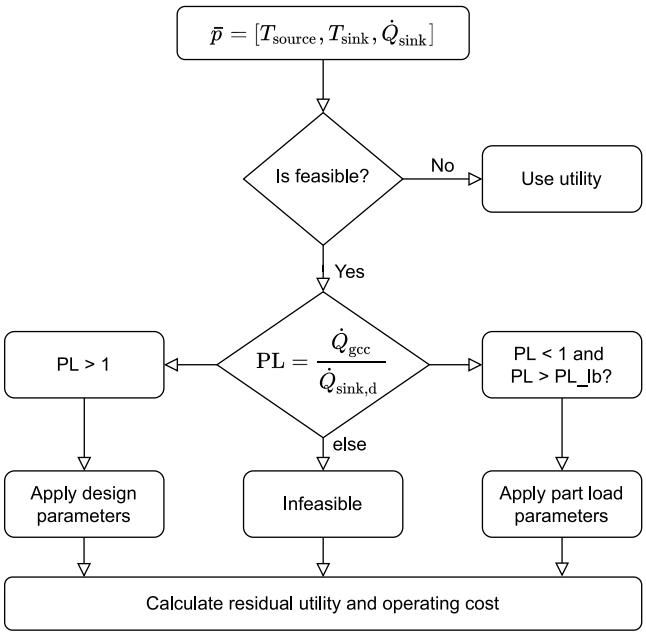

Fig. 7. Overview of the calculation order within the optimization.

an optimization variable. Furthermore, PL_{lb} can be used to constraint the technical feasible minimum load of the heat pump.

The heat pump is modelled through the previously described reduced-order part load model and evaluated by the fitted second-order polynomial.

However, if PL is greater than 1 the process requires more heat at T_{sink} than the design heat load of the heat pump, which means the heat pump does not have to operate in part load. Design conditions apply and residual utility and cost calculations are run.

3.3. Economic evaluation

The NPV is calculated according to Eq. (29). Where R_x are the cash flows in year x. The discount rate i and the investment lifetime N. It is assumed that both the interest rate and cash flows remain constant over the evaluation period.

$$\mathrm{NPV} = \sum_{x=0}^{N} \frac{R_x}{(1+i)^x} \tag{29}$$

The cash inflows of the NPV correspond to the savings s (Eq. (30)) realized in operating expenditures (OPEX) through the utilization of a heat pump for heat supply instead of conventional utility. Additionally, the initial capital expenditure (CAPEX) associated with the heat pump constitutes a negative cash inflow in the initial year. The specific economic parameters are depicted in Table 3.

$$\mathrm{s} = c_{\mathrm{opex,no\ hp}} - c_{\mathrm{opex,hp}} \tag{30}$$

In Walden et al. (2023b) several large-scale heat pump capital cost functions have been compared. The CAPEX of the heat pump is estimated by Eq. (31) proposed by Schlosser (2021) with the addition of an operation and maintenance factor of 1% of the CAPEX. The applied parameters within the cost function can be found in Table 3.

$$c_{\mathrm{inv}} = \mathrm{f_{HP}} \cdot \dot{Q}_{\mathrm{sink}}^{\mathrm{E_{HP}}} \cdot \mathrm{f_{PI}} \cdot \mathrm{f_{sys}} \cdot \mathrm{f_{om}} \tag{31}$$

Another important parameter for the evaluation of the heat pump is the heat coverage. The heat coverage determines the percentage of heat covered by the heat pump annually.

$$Q_{\mathrm{cov}} = \frac{\int_0^t \dot{Q}_{\mathrm{sink}}\, d\tau}{\int_0^t \dot{Q}_{\mathrm{HU}}\, d\tau} \cdot 100 \tag{32}$$

Table 3
Parameters for the economic evaluation.

	Value
c_{HU}	80 (€/MWh)
c_{CU}	40 (€/MWh)
c_{el}	160 (€/MWh)
n_{lifetime}	20 (y)
i	7 (%)
Parameters of CAPEX function	Schlosser (2021)
f_{HP}	$\begin{cases} 1521\,(€/\mathrm{kW_{th}}) & \text{if } \dot{Q}_{\mathrm{sink}} \le 210\,\mathrm{kW_{th}} \\ 349.5\,(€/\mathrm{kW_{th}}) & \text{if } \dot{Q}_{\mathrm{sink}} > 210\,\mathrm{kW_{th}} \end{cases}$
E_{HP}	$\begin{cases} 0.637 & \text{if } \dot{Q}_{\mathrm{sink}} \le 210\,\mathrm{kW_{th}} \\ 0.912 & \text{if } \dot{Q}_{\mathrm{sink}} > 210\,\mathrm{kW_{th}} \end{cases}$
f_{pi}	1.25 (–)
f_{sys}	1.8 (–)
f_{om}	1.01 (–)

4. Case study

The considered case study is the same as in the preceding research (Walden et al., 2023b) in order to show the impact of heat pump flexibility in process integration. The study is based on the process data of a transient simulation of a paintshop process similar to Giampieri et al. (2020). The study assumes continuous hourly operation over the entire year, covering all 8759 h in the simulated process data. Fluctuations in heating and cooling demands are predominantly influenced by weather conditions. Fig. 8 shows the processes individual hourly GCCs.

It should be noted that this study focuses on the targeting of heat pump integration based on the existing process demand states and thus it does not focus on the specifics of the underlying process.

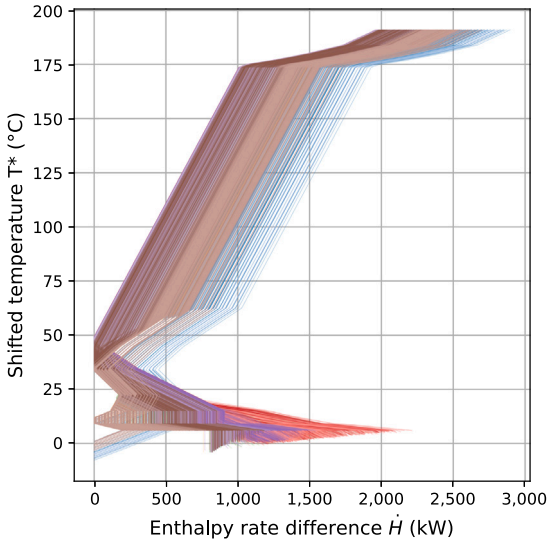

Fig. 8. Visualization of the Grand Composite Curves throughout the 8759 process states.
Source: The case study is taken from the authors previous work (Walden et al., 2023b).

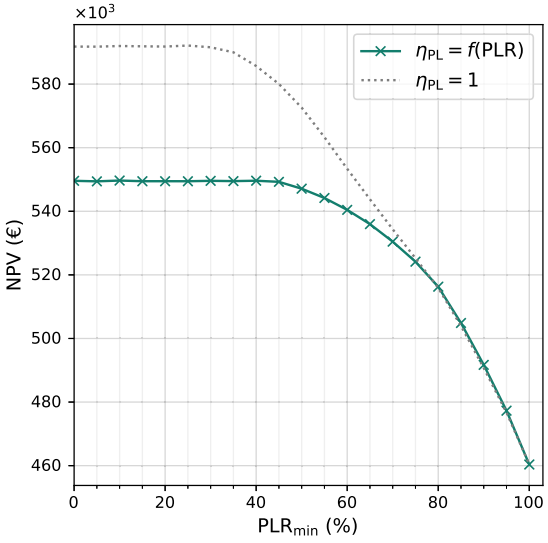

Fig. 9. The effect of the minimum part load ratio PLR$_{min}$ the NPV. The dotted grey line represents heat pump parameters with no part load efficiency change, while the solid line illustrates the NPV of heat pumps which have a altered efficiency when operating in part load. 100% PLR$_{min}$ represents a minimum load of 100% indicating a heat pump without load flexibility.

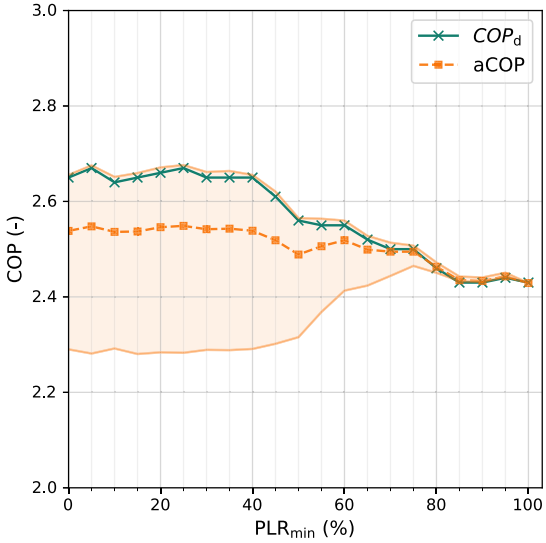

Fig. 10. Comparison of the design COP for different PLR$_{min}$ ratios. The shaded area indicates the operational range of the COP. aCOP is the annualized mean COP.

5. Results

The optimization methodology detailed in Section 3.2 is implemented in the context of the case study.

PLR$_{min}$ denotes the minimum relative load of the heat pump concerning its design load. If PLR$_{min}$ is set to 100%, the heat pump is only able to operate at the design heat sink heat load ($\dot{Q}_{sink,d}$). Analogous, a heat pump with a PLR$_{min}$ of 60% can operate as low as 60% of $\dot{Q}_{sink,d}$. Thus, it is capable of reducing its heating load by 40%. This means, it can operate at any heat load between 60% and 100% of $\dot{Q}_{sink,d}$.

A more flexible heat pump has different optimal integration point than a less load flexible one. Consequently, the heat pump integration parameters (T_{sink}, T_{source}, $\dot{Q}_{sink}$) are optimized and thus vary for each PLR$_{min}$ value. For example, a heat pump that is able to operate at 0.8 PLR$_{min}$ is likely to have different optimal parameters – which includes the integration parameters and the resulting parameters such as COP, coverage, cost – and a different integration point than a heat pump which is capable of 0.6 PLR$_{min}$.

Fig. 9 shows the effect on the NPV by decreasing the minimum part load ratio PLR$_{min}$ of the heat pump. In all Figures, the dotted grey line represents heat pump parameters assuming no efficiency change in part load, while the solid line illustrates the heat pump parameters incorporating the part load model described earlier (Section 2). An incremental enhancement in the achievable minimum part load ratio PLR$_{min}$ results in substantial NPV gains. However, in the investigated case study, values below 40% PLR$_{min}$ do not significantly enhance the investment's value. For example, a more flexible heat pump with a PLR$_{min}$ of 5% – meaning it can operate as low as 5% of its design heat load – does not provide an economical benefit over a heat pump with a PLR$_{min}$ of only 40%. The gains in heat pump load flexibility result in diminishing returns, indicating that further increases in load flexibility yield no improvements in the investment's value.

Fig. 10 depicts the design COP$_d$ as solid line and as shaded area, the COP range for each PLR$_{min}$. With increased flexibility, the optimal COP$_d$ increases. Which means, a heat pump with a higher flexibility is integrated with a different temperature lift. Thus, different heat source or heat sink temperatures. The annualized mean COP, aCOP, is always greater than the 100% PLR COP, which indicates one reason for the significantly improved NPV. However, similar to the NPV, the COP$_d$ converges at 40% PLR$_{min}$, which means additional flexibility potential is not required nor beneficial to achieve the optimal business case in the current case study.

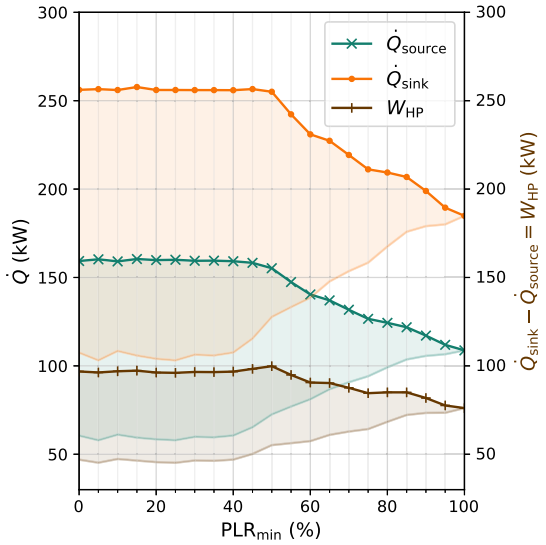

Fig. 11. The installed heat source and heat sink heat load of heat pumps with different operable minimum part load ratios PLR$_{min}$. The shaded area marks the operating span, while the solid line indicates the design value. The right side axis shows the heat pumps power, as can be derived from the energy balance (Eq. (1)).

In Fig. 11 the heating capacity of the heat source and heat sink is depicted. The heat pumps work input is visualized in a similar manner. The required work input for a heat pump can be determined based on its energy balance (Eq. (1)). The shaded area shows the operating range of the heat pumps heat load throughout the analysed year. With decreasing PLR$_{min}$, the heat pump is more load-flexible and thus, the operating range and shaded area is larger.

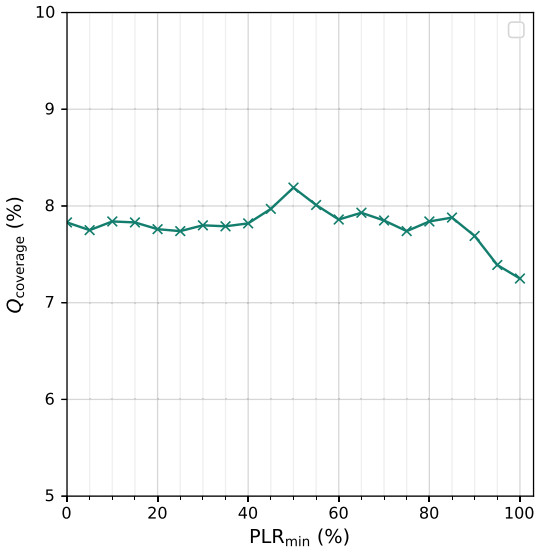

Fig. 12. Percentage of annual heat demand covered by the heat pumps over the feasible level of PLR_{min}.

For reference, the work of Meesenburg et al. (2020) showed that large changes in heat pump load are realizable within short time frames to provide ancillary service to the power grid. The work investigated a two-stage ammonia heat pump with a variable speed piston compressor for district heating.

The increase in heating capacity is anticipated, because a larger heat pump can be installed, which is still able to cover operating cases with a lower heat demand at the heat sink temperature. The installation of a larger heat pump, however, results in increased CAPEX, which ultimately leads to an economic limit in installed heating capacity. The ascending trend in heating capacity converges at 50% minimum load PLR_{min}, mirroring the trends observed in OPEX and NPV. A heat pump with a PLR_{min} set to 50% has an increased heating capacity $\dot{Q}_{sink}$ of an additional 70 kW compared to an optimal heat pump which only operates at full load, i.e. 100% PLR_{min}. In terms of relative percentage change, this corresponds to a 38% increase in installed heating capacity. Simultaneously, the heat source heating capacity experiences an enhancement, amounting to an additional 46 kW in heating capacity — an increase of 43%. Both installed heat loads increase nearly linear with PLR_{min}. The required heat pump power is increased by only 24 kW, which accounts to 31%. This efficiency gain is due to an increased COP as seen in Fig. 10.

An increase in the heat pumps heating capacity beyond 256 kW is not economically beneficial. This can be explained by the steep temperature glide of the process streams as seen in the GCC. Increasing the heat pumps heating capacity beyond 256 kW would require a higher temperature lift and consequently lower the COP, thus perform worse in OPEX. An abstraction between the inclination of the process stream $\frac{1}{\dot{m}c_p}$, the capacity of the heat pump and the operating cost is required. However, this is beyond the scope of this work.

However, a larger and more flexible heat pump is expected to enhance the heat coverage. Hence, Fig. 12 examines the influence of load flexibility on the annual heat coverage. The heat coverage is defined in Eq. (32) as the ratio of annual heat supplied by the heat pump and the total heat demand. A marginal increase in heat coverage is observed as the minimum feasible load decreases. This leads to the conclusion that the enhancements in NPV are not primarily driven by an increase in annual heat coverage, but by an increase in average annual efficiency as depicted in Fig. 10.

Another benefit of the proposed methodology is, that each heat pump parameter is evaluated at each hour throughout year and thus, can be analysed. Fig. 13 shows the operating COP over the entire operating range of 8759 h of different heat pumps which can achieve PLR_{min} of 30%, 70% and 90%, indicated by the colours. The solid line shows the design value, the dotted line the annual mean value and the transparent line visualizes the operational value at the corresponding time step. The visualization leads to three main observations as the PLR_{min} is lowered:

1. An increasing fluctuation in operational COP
2. A steadily growing design COP_d
3. Part load operation only occurs in summer and the transitional period

Observation (1) explains why a heat pump with PLR_{min} = 90% and no efficiency change in part load $\eta_{PL} = 1$ does not perform significantly better than a heat pump with part load efficiency losses (see dotted line in Fig. 9): because the heat pump rarely operates in part load. This can lead to marginal gains in efficiency (see Eq. (10)). On the other hand, a heat pump with a lower minimum load PLR_{min} has a larger heating capacity and thus, operates more frequently in part load. Operating more frequently in part load leads to decreases in efficiency. The data depicted in Fig. 13 shows that the annualized mean COP for a heat pump with a higher PLR_{min} is significantly lower than its design COP. This is not the case for less flexible heat pumps. However, it should be noted that the COP never drops below the electricity to reference fuel price ratio (Eq. (24)) of 2 and thus, never operates economically unfavourable. Observation (2) confirms the described behaviour in Fig. 10.

Fig. 14 shows a load-duration curve of the heat pumps heat flow rate at the heat sink. A load-duration curve visualizes the energy demand against the duration for which the demand occurs. The 100% PLR_{min} heat pump clearly shows an operation only at the design heat flow rate spanning over the operating hours. As the achievable minimum load is stepwise increased to 0%, the heat pumps show a higher heat load for the majority of operating hours and flexible heat loads beyond 4000 operating hours. This behaviour is increasing constantly. However, as previously highlighted, the heat pumps with a PLR_{min} below 40% do not show any change in trend and overlap in the load-duration curve.

Furthermore, the integral of the load-duration curve is the heat covered throughout the analysed time period. The area for the non-flexible heat pump and the increasingly load flexible heat pumps are roughly equal, as demonstrated in Fig. 12. Thus, in the analysed case, the main economic benefit of a load flexible heat pump is the increased efficiency in COP by a reduced temperature lift while maintaining the same heat coverage of the process heat demand.

Fig. 15 explores the impact of various heat pump integrations on the NPV resulting from increased load flexibility potential. It is evident that a higher heat pump Carnot efficiency η_{carnot} substantially elevates the NPV. However, the Figure shows that the heat pumps minimum load PLR_{min} has a greater impact on the NPV of the heat pump integration when η_{carnot} is lower. The optimum NPV for a heat pump with a 40% η_{carnot} is achieved at a 40% PLRmin, while a heat pump with a 60% η_{carnot} reaches its NPV peak at 85% PLR_{min}. This implies that a more efficient heat pump does not necessitate the same level of flexibility as a less efficient heat pump to attain its most advantageous integration and performance. It should be mentioned, that this might vary depending on the underlying boundary conditions and process.

6. Conclusion

The present work proposes a reduced order part load heat pump model and addresses the impact of heat pump load flexibility on its process integration and design parameters.

The findings of the case study reveal that a flexibility threshold exists, beyond which part load operation leads to diminishing returns.

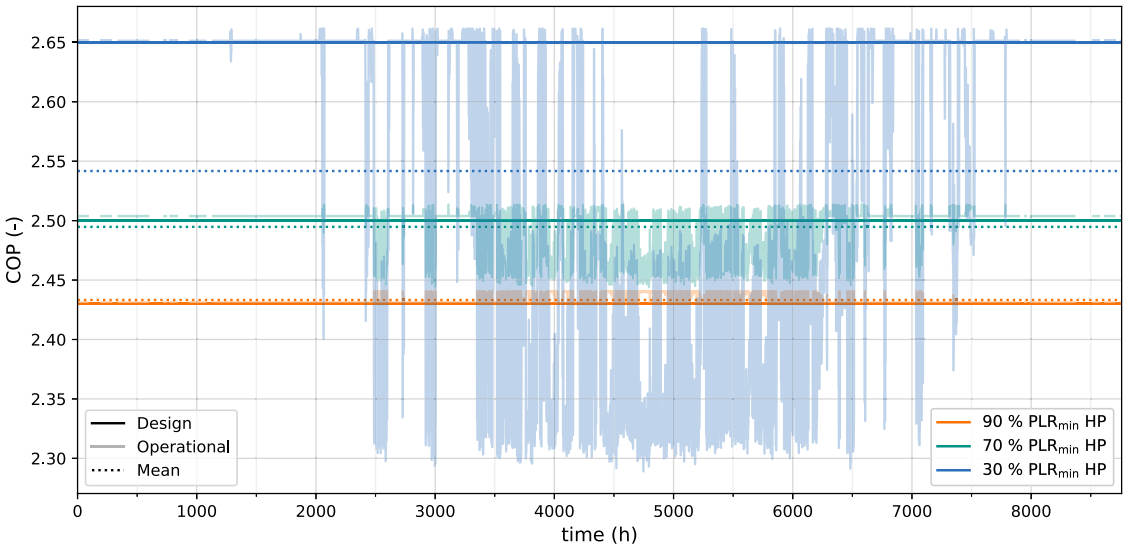

Fig. 13. Annual behaviour of the COP for the different heat pump integrations which can achieve a minimum load PLR_{min} of 30%, 70% and 90%. The straight lines indicate the design COP_d, while the shaded lines show the operational COP at each hour. The dotted line indicates the annualized mean COP. It should be noted, that infeasible heat pump operating cases are not displayed.

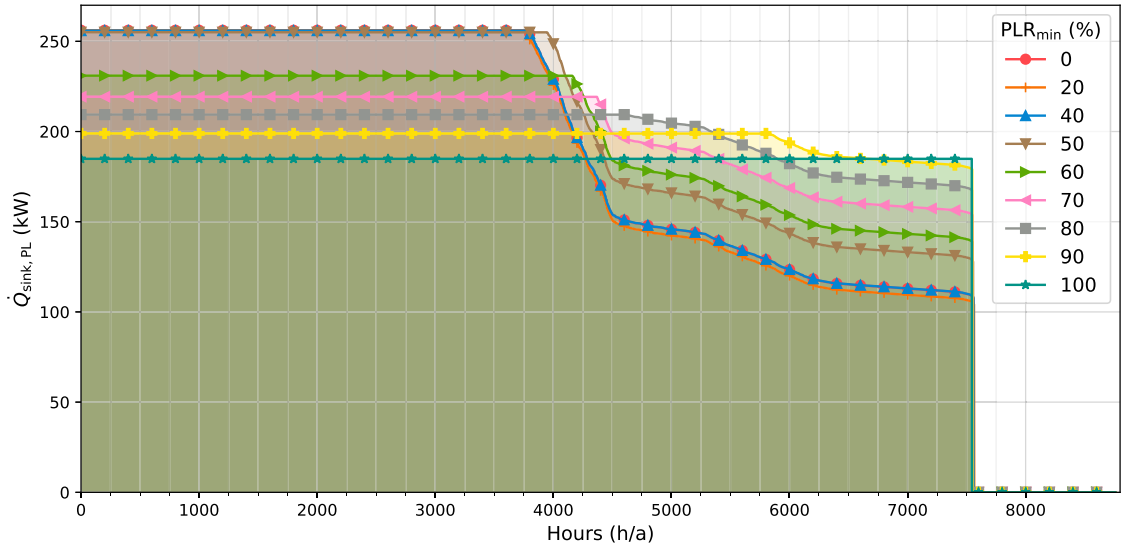

Fig. 14. A load-duration curve for the heat sink heat load of the heat pumps. Different colours and markers visualize heat pumps with different minimum loads PLR_{min}.

In the specific context of this study, this threshold is identified at a minimum load of 45%. The capacity for load flexibility up to this threshold corresponds to a 19% increase in the Net Present Value (NPV) of the investment. Furthermore, it was found that increasing the minimum part load ratio does not increase the annual heat coverage by the heat pump while maximizing net present value. Instead, a comparable level of heat coverage is maintained, accompanied by an increase in Coefficient of Performance and heating capacity of the heat pump.

Additionally, the Carnot efficiency of a heat pump reduces the dependency on flexibility for achieving optimal investment returns for the investigated case study. These insights emphasize the importance of carefully balancing load flexibility, system size, and efficiency to achieve optimal heat pump performance and economic viability. However, it should be noted, that the efficiency and heat pump parameter trends may differ depending on the investigated case study.

The present work inspires a variety of ideas for future work. The implementation of a multi-objective optimization appears promising for enhancing both the annual heat coverage rate and flexibility in the context of economical decarbonization.

Furthermore, a generalization on the connection between the economically-optimal heat pump integration parameters and the process stream temperature glide would be highly advantageous. Such a generalization could find broad utilization as it would be universally applicable.

Table A.1
Result dataset.

PLR_{min} (%)	T_{source} (°C)	T_{sink} (°C)	$\dot{Q}_{sink}$ (kW)	$\dot{Q}_{source}$ (kW)	COP (–)	P (kW)	T_{lift} (°C)	NPV (k€)	OPEX (k€)	CAPEX (k€)	Op. hours (h)	Q_{cov} (%)
0.0	17.2	68.9	256.1	159.3	2.6	96.8	51.7	549.6	1760.5	123.6	7558.0	7.8
5.0	17.1	68.4	256.5	160.3	2.7	96.3	51.3	549.4	1760.5	123.8	7557.0	7.8
10.0	17.2	69.1	256.0	159.1	2.6	97.0	51.8	549.7	1760.5	123.6	7559.0	7.8
15.0	17.1	68.7	257.7	160.4	2.6	97.3	51.6	549.5	1760.4	124.3	7558.0	7.8
20.0	17.1	68.5	256.1	159.8	2.7	96.2	51.4	549.5	1760.5	123.6	7563.0	7.8
25.0	17.1	68.4	256.1	160.0	2.7	96.0	51.2	549.4	1760.5	123.6	7561.0	7.7
30.0	17.2	68.8	256.0	159.4	2.6	96.5	51.6	549.6	1760.5	123.6	7558.0	7.8
35.0	17.2	68.7	256.0	159.5	2.6	96.5	51.5	549.5	1760.5	123.6	7557.0	7.8
40.0	17.2	69.0	255.9	159.2	2.6	96.8	51.7	549.6	1760.5	123.6	7559.0	7.8
45.0	17.3	69.8	256.6	158.3	2.6	98.3	52.6	549.3	1760.5	123.8	7556.0	8.0
50.0	17.5	71.4	255.1	155.2	2.6	99.8	53.9	547.1	1760.8	123.2	7555.0	8.2
55.0	18.0	72.0	242.3	147.4	2.5	94.9	54.1	544.2	1761.6	117.5	7556.0	8.0
60.0	18.4	72.7	231.0	140.4	2.5	90.6	54.2	540.4	1762.4	112.5	7551.0	7.9
65.0	18.6	73.8	227.3	137.1	2.5	90.3	55.1	536.0	1763.0	110.9	7546.0	7.9
70.0	19.0	74.5	219.3	131.7	2.5	87.6	55.5	530.5	1763.9	107.3	7550.0	7.8
75.0	19.3	75.1	211.2	126.6	2.5	84.5	55.8	524.1	1764.8	103.7	7548.0	7.7
80.0	19.5	76.2	209.4	124.3	2.5	85.0	56.8	516.3	1765.6	103.0	7546.0	7.8
85.0	19.6	77.2	206.8	121.8	2.4	85.0	57.6	504.9	1766.8	102.2	7544.0	7.9
90.0	19.9	77.6	198.9	117.1	2.4	81.8	57.7	491.7	1768.2	99.7	7548.0	7.7
95.0	20.2	77.7	189.5	111.9	2.4	77.6	57.5	477.3	1769.9	96.6	7544.0	7.4
100.0	20.5	78.3	184.9	108.8	2.4	76.1	57.9	460.4	1771.6	95.1	7544.0	7.2

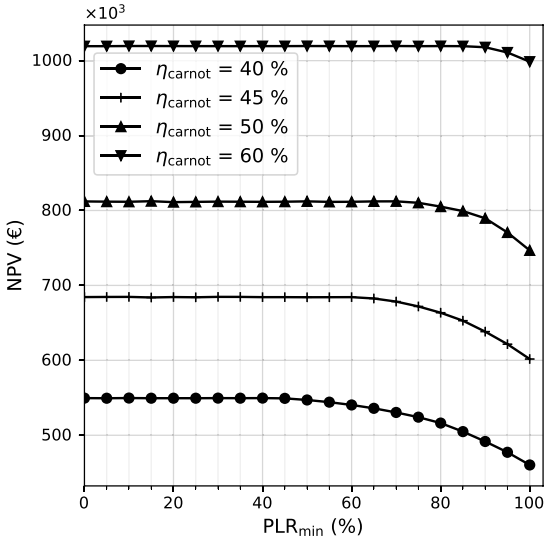

Fig. 15. The impact of the Carnot efficiency on the economics of heat pump flexibility.

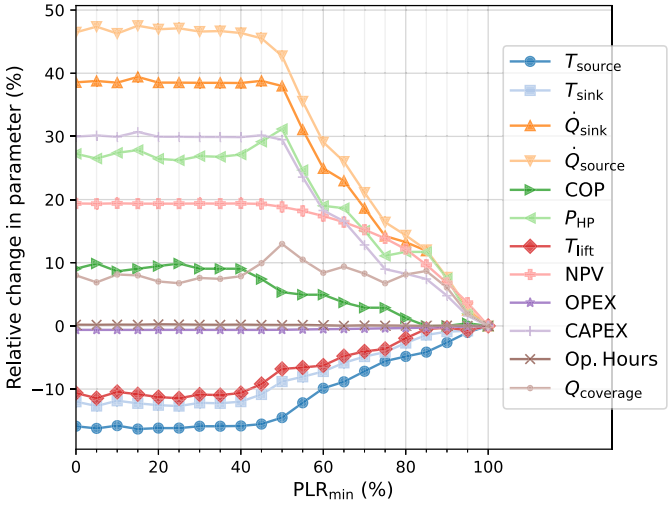

Fig. B.1. Relative change of heat pump and economic parameters with a lower relative minimum load PLR_{min}.

CRediT authorship contribution statement

Jasper V.M. Walden: Writing – review & editing, Writing – original draft, Visualization, Validation, Software, Methodology, Investigation, Formal analysis, Data curation, Conceptualization. **Panagiotis Stathopoulos:** Writing – review & editing, Supervision.

Declaration of competing interest

The authors declare that they have no known competing financial interests or personal relationships that could have appeared to influence the work reported in this paper.

Data availability

Data will be made available on request.

Acknowledgements

The author would like to thank Jens Gollasch and Phong Tran for their valuable feedback and insights. The authors declare no competing interests. This research did not receive any specific grant from funding agencies in the public, commercial, or not-for-profit sectors.

Appendix

Supplementary data on this article are given below.

Appendix A. Result dataset

The results of the optimizations are displayed in Table A.1.

Appendix B. Relative change in parameters with PLR_{min}

Fig. B.1 displays the relative change of each parameter for an optimized integration for each value of minimum part load PLR_{min}. Where 100% PLR_{min} is the case in which the heat pump is only operable at 100% load.

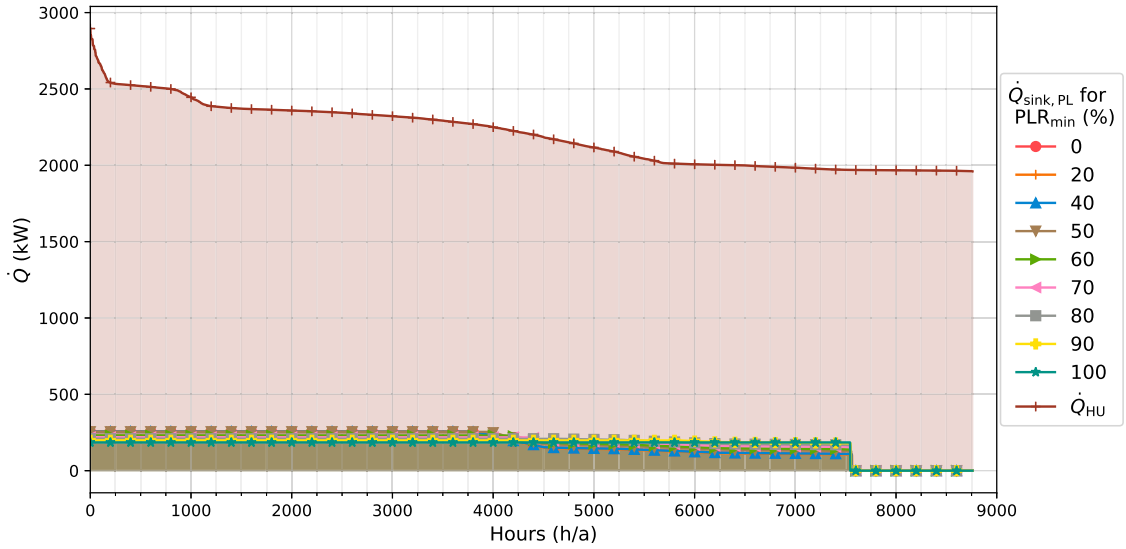

Fig. C.1. Load-duration curve for the process total heat demand over the investigated time horizon. The heat pumps heat sink heat loads are for heat pumps with different capabilities for load flexibility.

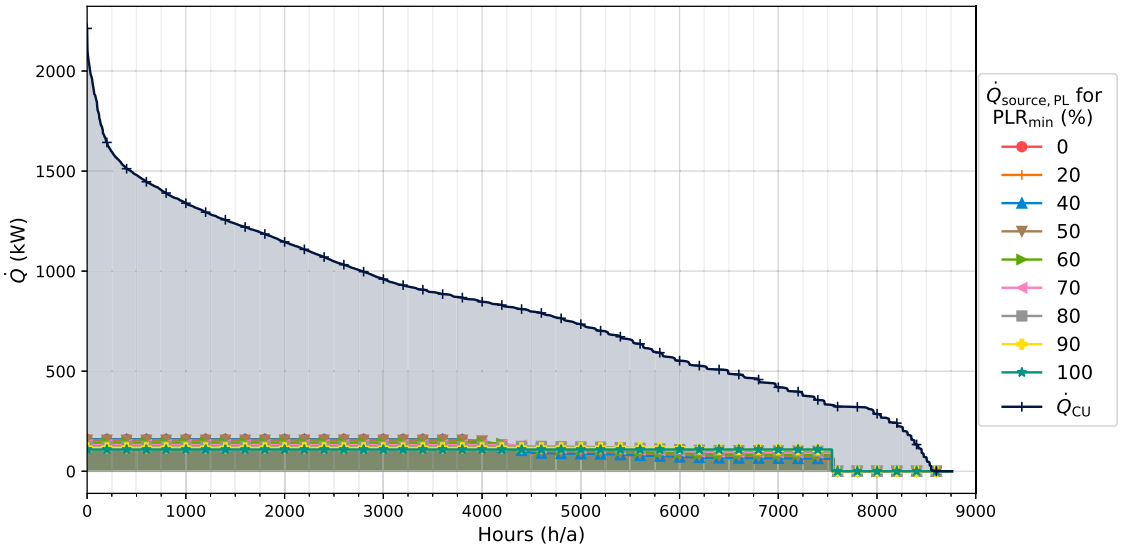

Fig. C.2. Load-duration curve for the process total cooling demand over the investigated time horizon. The heat pumps heat source heat loads are visualized for heat pumps with different capabilities for load flexibility.

Appendix C. Load-duration curves for process heating and cooling requirement

Fig. C.1 shows the load-duration curve of the process total heat demand. Furthermore, Fig. C.1 has been added to show the heat sink heat loads of the heat pumps in the context of the process heat demand. However, this Figure should be interpreted cautiously as it does not visualize the temperature glide of the heat demand.

Analogous, Fig. C.2 shows the process total cooling demand in a load-duration curve. In this Figure, the heat source heat load of the heat pumps are also visualized for different load flexible heat pumps, with different PLR_{min} values.

References

Adamson, K.-M., Walmsley, T.G., Carson, J.K., Chen, Q., Schlosser, F., Kong, L., Cleland, D.J., 2022. High-temperature and transcritical heat pump cycles and advancements: A review. Renew. Sustain. Energy Rev. 167, 112798. http://dx.doi.org/10.1016/j.rser.2022.112798.

Agner, R., Ong, B.H.Y., Stampfli, J.A., Krummenacher, P., Wellig, B., 2022. A graphical method for combined heat pump and indirect heat recovery integration. Energies 15 (8), 2829. http://dx.doi.org/10.3390/en15082829.

Aguilera, J.J., Meesenburg, W., Ommen, T., Markussen, W.B., Poulsen, J.L., Zühlsdorf, B., Elmegaard, B., 2022. A review of common faults in large-scale heat pumps. Renew. Sustain. Energy Rev. 168, 112826. http://dx.doi.org/10.1016/j.rser.2022.112826.

AHRI - Air-Conditioning, Heating, and Refrigeration Institute, 2020. Standard 210/240: Performance rating of unitary air-conditioning & air-source heat pump equipment.

Ayub, Z.H., Khan, T.S., Salam, S., Nawaz, K., Ayub, A.H., Khan, M.S., 2019. Literature survey and a universal evaporation correlation for plate type heat exchangers. Int. J. Refrig. 99, 408–418. http://dx.doi.org/10.1016/j.ijrefrig.2018.09.008.

Becker, H., Vuillermoz, A., Maréchal, F., 2012. Heat pump integration in a cheese factory. Appl. Therm. Eng. 43, 118–127. http://dx.doi.org/10.1016/j.applthermaleng.2011.11.050.

Cecchinato, L., 2010. Part load efficiency of packaged air-cooled water chillers with inverter driven scroll compressors. Energy Convers. Manage. 51 (7), 1500–1509. http://dx.doi.org/10.1016/j.enconman.2010.02.008.

Chen, J.C., 1966. Correlation for boiling heat transfer to saturated fluids in convective flow. Ind. Eng. Chem. Process Des. Dev. 5 (3), 322–329. http://dx.doi.org/10.1021/i260019a023.

Crosser, O.K., 1955. Condensing Heat Transfer Within Horizontal Tubes. Rice University.

Deymi-Dashtebayaz, M., Farahnak, M., Abadi, R.N.B., 2019. Energy saving and environmental impact of optimizing the number of condenser fans in centrifugal chillers under partial load operation. Int. J. Refrig. 103, 163–179. http://dx.doi.org/10.1016/j.ijrefrig.2019.03.020.

Dittus, F.W., Boelter, L., 1985. Heat transfer in automobile radiators of the tubular type. Int. Commun. Heat Mass Transfer 12 (1), 3–22. http://dx.doi.org/10.1016/0735-1933(85)90003-X.

Dorao, C.A., Fernandino, M., 2017. Dominant dimensionless groups controlling heat transfer coefficient during flow condensation inside pipes. Int. J. Heat Mass Transfer 112, 465–479. http://dx.doi.org/10.1016/j.ijheatmasstransfer.2017.04.104.

Eiholzer, T., Olsen, D., Hoffmann, S., Sturm, B., Wellig, B., 2017. Integration of a solar thermal system in a medium-sized brewery using pinch analysis: Methodology and case study. Appl. Therm. Eng. 113, 1558–1568. http://dx.doi.org/10.1016/j.applthermaleng.2016.09.124.

Gerard, F., Opinska, L.G., Smit, T., Rademaekers, K., Braungardt, S., Monejar Montagud, M.E., 2021. Policy support for heating and cooling decarbonisation. URL https://op.europa.eu/o/opportal-service/download-handler?identifier=f5118ffc-eabd-11ec-a534-01aa75ed71a1&format=pdf&language=en&productionSystem=cellar&part=.

Ghaderi, M., Hosseinnia, S.M., Sorin, M., 2023. Assessment of waste heat recovery potential in greenhouse ventilation systems using dynamic pinch analysis. Appl. Therm. Eng. 227, 120363. http://dx.doi.org/10.1016/j.applthermaleng.2023.120363.

Giampieri, A., Ling-Chin, J., Ma, Z., Smallbone, A., Roskilly, A.P., 2020. A review of the current automotive manufacturing practice from an energy perspective. Appl. Energy 261, 114074. http://dx.doi.org/10.1016/j.apenergy.2019.114074.

Han, D., Moon, C., Park, C., Lee, K.-J., 2006. Condensation heat transfer correlation for smooth tubes in annular flow regime. J. Mech. Sci. Technol. 20 (8), 1275–1283. http://dx.doi.org/10.1007/BF02916027.

IEA HPT Annex 58, 2023. High-temperature heat pumps: Task 1 - technologies.

Incropera, F.P., 2007. Fundamentals of Heat and Mass Transfer, sixth ed. Wiley, Hoboken, NJ.

Jiang, J., Hu, B., Wang, R.Z., Deng, N., Cao, F., Wang, C.-C., 2022. A review and perspective on industry high-temperature heat pumps. Renew. Sustain. Energy Rev. 161, 112106. http://dx.doi.org/10.1016/j.rser.2022.112106.

Klinac, E., Carson, J.K., Hoang, D., Chen, Q., Cleland, D.J., Walmsley, T.G., 2023. Multi-level process integration of heat pumps in meat processing. Energies 16 (8), 3424. http://dx.doi.org/10.3390/en16083424.

Kosmadakis, G., 2019. Estimating the potential of industrial (high-temperature) heat pumps for exploiting waste heat in EU industries. Appl. Therm. Eng. 156, 287–298. http://dx.doi.org/10.1016/j.applthermaleng.2019.04.082.

Li, Y., Zhang, G., Wang, L., Yang, Y., 2020. Part-load performance analysis of a combined cycle with intermediate recuperated gas turbine. Energy Convers. Manage. 205, 112346. http://dx.doi.org/10.1016/j.enconman.2019.112346.

Lin, H.-Y., M, M., Yang, C.-M., Nawaz, K., Wang, C.-C., 2023. Universal correlation for falling film evaporation on a horizontal plain tube. Int. J. Refrig. 146, 261–273. http://dx.doi.org/10.1016/j.ijrefrig.2022.11.006.

Lincoln, B.J., Kong, L., Pineda, A.M., Walmsley, T.G., 2022. Process integration and electrification for efficient milk evaporation systems. Energy 258, 124885. http://dx.doi.org/10.1016/j.energy.2022.124885.

Madeddu, S., Ueckerdt, F., Pehl, M., Peterseim, J., Lord, M., Kumar, K.A., Krüger, C., Luderer, G., 2020. The CO 2 reduction potential for the European industry via direct electrification of heat supply (power-to-heat). Environ. Res. Lett. 15 (12), 124004. http://dx.doi.org/10.1088/1748-9326/abbd02.

Marina, A., Spoelstra, S., Zondag, H.A., Wemmers, A.K., 2021. An estimation of the European industrial heat pump market potential. Renew. Sustain. Energy Rev. 139, 110545. http://dx.doi.org/10.1016/j.rser.2020.110545.

Meesenburg, W., Markussen, W.B., Ommen, T., Elmegaard, B., 2020. Optimizing control of two-stage ammonia heat pump for fast regulation of power uptake. Appl. Energy 271, 115126. http://dx.doi.org/10.1016/j.apenergy.2020.115126.

Meesenburg, W., Ommen, T., Elmegaard, B., 2018. Dynamic exergoeconomic analysis of a heat pump system used for ancillary services in an integrated energy system. Energy 152, 154–165. http://dx.doi.org/10.1016/j.energy.2018.03.093.

Olsen, D., Liem, P., Abdelouadoud, Y., Wellig, B., 2017. Thermal energy storage integration based on pinch analysis - methodology and application. Chem. Ing. Tech. 89 (5), 598–606. http://dx.doi.org/10.1002/cite.201600103.

Padullés, R., Hansen, M.L., Andersen, M.P., Jensen, J.K., Elmegaard, B., Zühlsdorf, B., 2023. Potential for optimal operation of industrial heat pumps with thermal energy storage for emissions and cost reduction. In: Smith, J.R. (Ed.), 36th International Conference on Efficiency, Cost, Optimization, Simulation and Environmental Impact of Energy Systems. ECOS 2023, ECOS 2023, Las Palmas De Gran Canaria, Spain, pp. 2194–2205. http://dx.doi.org/10.52202/069564-0198.

Prendl, L., Schenzel, K., Hofmann, R., 2021. Simultaneous integration of heat pumps and different thermal energy storages into a tightened multi-period MILP HENS superstructure formulation for industrial applications. Comput. Chem. Eng. 147, 107237. http://dx.doi.org/10.1016/j.compchemeng.2021.107237.

Sadjjadi, B.S., Gerdes, J.-N., Sauer, A., 2023. Energy flexible heat pumps in industrial energy systems: A review. Energy Rep. 9, 386–394. http://dx.doi.org/10.1016/j.egyr.2022.12.110.

Salimpour, M.R., 2009. Heat transfer coefficients of shell and coiled tube heat exchangers. Exp. Therm Fluid Sci. 33 (2), 203–207. http://dx.doi.org/10.1016/j.expthermflusci.2008.07.015.

Schlosser, F., 2021. Integration von Wärmepumpen zur Dekarbonisierung der Industriellen Wärmeversorgung. Kassel University Press, http://dx.doi.org/10.17170/KOBRA-202103023389.

Schlosser, F., Arpagaus, C., Walmsley, T.G., 2019. Heat pump integration by pinch analysis for industrial applications: A review. Chem. Eng. Trans. (76), 7–12. http://dx.doi.org/10.3303/CET1976002.

Schlosser, F., Jesper, M., Vogelsang, J., Walmsley, T.G., Arpagaus, C., Hesselbach, J., 2020. Large-scale heat pumps: Applications, performance, economic feasibility and industrial integration. Renew. Sustain. Energy Rev. 133, 110219. http://dx.doi.org/10.1016/j.rser.2020.110219.

Schlosser, F., Zysk, S., Walmsley, T.G., Kong, L., Zühlsdorf, B., Meschede, H., 2023. Break-even of high-temperature heat pump integration for milk spray drying. Energy Convers. Manage. 291, 117304. http://dx.doi.org/10.1016/j.enconman.2023.117304.

Shah, M.M., 1979. A general correlation for heat transfer during film condensation inside pipes. Int. J. Heat Mass Transfer 22 (4), 547–556. http://dx.doi.org/10.1016/0017-9310(79)90058-9.

Shah, M.M., 2021a. A general correlation for heat transfer during evaporation of falling films on single horizontal plain tubes. Int. J. Refrig. 130, 424–433. http://dx.doi.org/10.1016/j.ijrefrig.2021.04.025.

Shah, M.M., 2021b. Prediction of heat transfer in evaporation of saturated falling films on bundles of horizontal tubes. Int. J. Refrig. 131, 416–425. http://dx.doi.org/10.1016/j.ijrefrig.2021.07.004.

Stampfli, J.A., Atkins, M.J., Olsen, D.G., Walmsley, M.R., Wellig, B., 2019. Practical heat pump and storage integration into non-continuous processes: A hybrid approach utilizing insight based and nonlinear programming techniques. Energy 182, 236–253. http://dx.doi.org/10.1016/j.energy.2019.05.218.

Storn, R., Price, K., 1997. Differential evolution – A simple and efficient heuristic for global optimization over continuous spaces. J. Global Optim. 11 (4), 341–359. http://dx.doi.org/10.1023/A:1008202821328.

Thome, J.R., 2005. Condensation in plain horizontal tubes: recent advances in modelling of heat transfer to pure fluids and mixtures. J. Braz. Soc. Mech. Sci. Eng. 27 (1), http://dx.doi.org/10.1590/S1678-58782005000100002.

Towler, G., 2012. Chemical Engineering Design: Principles, Practice, and Economics of Plant and Process Design, second ed. Butterworth-Heinemann, Oxford and Waltham, MA, URL http://site.ebrary.com/lib/alltitles/Doc?id=10562149.

Townsend, D.W., Linnhoff, B., 1983. Heat and power networks in process design. Part I: Criteria for placement of heat engines and heat pumps in process networks. AIChE J. 29 (5), 742–748. http://dx.doi.org/10.1002/aic.690290508.

Turton, R., Bailie, R.C., Whiting, W.B., Shaeiwitz, J.A., Bhattacharyya, D., 2012. Analysis, Synthesis, and Design of Chemical Processes, fourth ed. In: Prentice Hall International Series in the Physical and Chemical Engineering Sciences, Prentice Hall, Upper Saddle River, N.J. and Munich.

Virtanen, P., Gommers, R., Oliphant, T.E., Haberland, M., Reddy, T., Cournapeau, D., Burovski, E., Peterson, P., Weckesser, W., Bright, J., van der Walt, S.J., Brett, M., Wilson, J., Millman, K.J., Mayorov, N., Nelson, A.R.J., Jones, E., Kern, R., Larson, E., Carey, C.J., Polat, VanderPlas, Jake, Laxalde, D., Perktold, J., Cimrman, R., Henriksen, I., Quintero, E.A., Harris, C.R., Archibald, A.M., Ribeiro, A.H., Pedregosa, F., van Mulbregt, P., SciPy 1.0 Contributors, 2020. SciPy 1.0: Fundamental algorithms for scientific computing in python. Nature Methods 17, 261–272. http://dx.doi.org/10.1038/s41592-019-0686-2.

Walden, J.V., Bähr, M., Glade, A., Gollasch, J., Tran, A.P., Lorenz, T., 2023a. Nonlinear operational optimization of an industrial power-to-heat system with a high temperature heat pump, a thermal energy storage and wind energy. Appl. Energy 344, 121247. http://dx.doi.org/10.1016/j.apenergy.2023.121247.

Walden, J.V., Wellig, B., Stathopoulos, P., 2023b. Heat pump integration in non-continuous industrial processes by dynamic pinch analysis targeting. Appl. Energy 352, 121933. http://dx.doi.org/10.1016/j.apenergy.2023.121933.

Walmsley, T.G., Klemes, J.J., Walmsley, M., Atkins, M.J., Varbanov, P.S., 2017. Innovative hybrid heat pump for dryer process integration. Chem. Eng. Trans. 57, 1039–1044. http://dx.doi.org/10.3303/CET1757174, URL https://www.cetjournal.it/index.php/cet/article/view/CET1757174.

Witte, F., Tuschy, I., 2020. TESPy: Thermal engineering systems in python. J. Open Source Softw. 5 (49), 2178. http://dx.doi.org/10.21105/joss.02178.

Zühlsdorf, B., Bühler, F., Bantle, M., Elmegaard, B., 2019a. Analysis of technologies and potentials for heat pump-based process heat supply above 150 °C. Energy Convers. Manag.: X 2, 100011. http://dx.doi.org/10.1016/j.ecmx.2019.100011.

Zühlsdorf, B., Jensen, J.K., Elmegaard, B., 2019b. Heat pump working fluid selection—economic and thermodynamic comparison of criteria and boundary conditions. Int. J. Refrig. 98, 500–513. http://dx.doi.org/10.1016/j.ijrefrig.2018.11.034.